Received: 9 February 2023 | Revised: 9 March 2023 | Accepted: 17 March 2023

DOI: 10.1002/msd2.12070

RESEARCH ARTICLE

IJMSD International Journal of Mechanical System Dynamics Open Access WILEY

Multiple control of thermoelectric dual-function metamaterials

Pengfei Zhuang | Jiping Huang

Department of Physics, State Key Laboratory of Surface Physics, Key Laboratory of Micro and Nano Photonic Structures (MOE), Fudan University, Shanghai, China

Correspondence
Prof. Jiping Huang, State Key Laboratory of Surface Physics, Key Laboratory of Micro and Nano Photonic Structures (MOE), Department of Physics, Fudan University, Shanghai 200438, China.
Email: jphuang@fudan.edu.cn

Funding information
National Natural Science Foundation of China, Grant/Award Number: 12035004; Science and Technology Commission of Shanghai Municipality, Grant/Award Number: 20JC1414700

Abstract

Thermal metamaterials based on transformation theory offer a practical design for controlling heat flow by engineering spatial distributions of material parameters, implementing interesting functions such as cloaking, concentrating, and rotating. However, most existing designs are limited to serving a single target function within a given physical domain. Here, we analytically prove the form invariance of thermoelectric (TE) governing equations, ensuring precise controls of the thermal flux and electric current. Then, we propose a dual-function metamaterial that can concentrate (or cloak) and rotate the TE field simultaneously. In addition, we introduce two practical control methods to realize corresponding functions: one is a temperature-switching TE rotating concentrator cloak that can switch between cloaking and concentrating; the other is an electrically controlled TE rotating concentrator that can handle the temperature field precisely by adjusting external voltages. The theoretical predictions and finite-element simulations agree well with each other. This work provides a unified framework for manipulating the direction and density of the TE field simultaneously and may contribute to the study of thermal management, such as thermal rectification and thermal diodes.

KEYWORDS

transformation thermotics, thermoelectric effect, dual-function thermal metamaterials, thermal management

1 | INTRODUCTION

Because heat energy is ubiquitous in nature, it is particularly important to control heat flow. Fortunately, various types of thermal metamaterials[1–3] based on the theory of transformation thermotics are emerging to meet the increasing demands of field manipulation. Thermal rotator[4,5] and concentrator[6–17] (cloak),[18–22] representative devices to control the direction and density of heat flux, travel through the research history of metamaterials. Nonetheless, there is no unified theoretical framework that accounts for the thermal rotator and concentrator at the same time.

On the other hand, it is important to address the problem that traditional metamaterials only serve single-target applications. Recently, multifunctional metamaterials[23–28] under the thermoelectric (TE) coupling field have been proposed, which is expected to pave the way for new approaches. However, most of the investigations neglect the regulating effect of the electric field itself on the thermal field. It is well known that the Peltier effect (one of the TE effects)[29–34] can convert electrical energy into heat due to the electron transfer of heat energy between two different materials. The electron releases (absorbs) heat to the outside world as it moves from a region of high (low) energy level to a region of low (high) energy level. Inspired by this concept, the electric field can be treated as a tunable parameter[35] to manipulate the thermal field.

In this work, we prove the form invariance of the TE coupling and derive the transformation relationship of constitutive parameters. Then, we establish a general framework to regulate the direction and density of heat flux (electric current) in a given region. Based on this framework, we design a dual-function metamaterial that can concentrate (or cloak) and rotate the TE field at the same time. To further control the TE field, we first introduce a temperature-dependent conductivity[36–45] with a step function, with the ability to switch between a rotating concentrator and cloak. In addition, we can not only manipulate the distribution of electric potential but also use the external electric potential as a means of regulating the thermal field. By adjusting the difference in external voltage, we can precisely control the temperature in the core–shell structure. These methods are demonstrated by finite-element simulation and achieve the desired effect. From an experimental point of view, the methods can be implemented by layer structure and shape memory alloys.[46,47] This work provides a broad platform for the manipulation of multiple physical fields and may inspire the research of thermal management devices such as thermal rectification[48,49] and diodes.[36,50]

2 | TRANSFORMATION TE THEORY

In this work, we consider a steady-state TE transport process, satisfying

$$\begin{cases} 0 = \nabla\cdot J_E, \\ 0 = \nabla\cdot J_Q + \nabla\mu\cdot J_E. \end{cases} \tag{1}$$

The heat flux J_Q and current J_E are, respectively, generated by Seeback and Peltier effect, that is,

$$\begin{cases} J_E = -\boldsymbol{\sigma}\nabla\mu - \boldsymbol{\sigma}\boldsymbol{S}\nabla T, \\ J_Q = -\boldsymbol{\kappa}\nabla T + T\boldsymbol{S}^{\mathrm{T}}J_E, \end{cases} \tag{2}$$

where T and $\mu$are the position-related temperature and electrical potential, respectively. The electric conductivity $\boldsymbol{\sigma}$, thermal conductivity $\boldsymbol{\kappa}$, and Seeback coefficient $\boldsymbol{S}$($\boldsymbol{S}^{\mathrm{T}}$ is the transpose of $\boldsymbol{S}$) are second-order tensors. By substituting Equation (2) into Equation (1), one has

$$\begin{cases} 0 = \nabla\cdot(\boldsymbol{\sigma}\nabla\mu + \boldsymbol{\sigma}\boldsymbol{S}\nabla T), \\ 0 = \nabla\cdot[\boldsymbol{\kappa}\nabla T + T\boldsymbol{S}^{\mathrm{T}}\boldsymbol{\sigma}\boldsymbol{S}\nabla T + T\boldsymbol{S}^{\mathrm{T}}\boldsymbol{\sigma}\nabla\mu] + \nabla\mu\cdot[\boldsymbol{\sigma}\nabla\mu + \boldsymbol{\sigma}\boldsymbol{S}\nabla T]. \end{cases} \tag{3}$$

Equation (3) summarizes the form of the TE equation in all coordinate systems but lacks many details. Therefore, we need to rewrite this equation into component forms for further comparisons. Without loss of generality, we consider an arbitrary coordinate system, consisting of a set of contravariant basis $\{\boldsymbol{g}^1, \boldsymbol{g}^2, \boldsymbol{g}^3\}$, a set of covariant basis $\{\boldsymbol{g}_1, \boldsymbol{g}_2, \boldsymbol{g}_3\}$, and corresponding contravariant components $\{x^1, x^2, x^3\}$. Based on this, the component form of Equation (3) can be expressed as

$$\begin{cases} 0 = \dfrac{1}{\sqrt{g}}\partial_u\left[\sqrt{g}\left(\sigma^u_l g^{lv}\partial_v\mu + \sigma^u_k S^k_l g^{lv}\partial_v T\right)\right], \\ 0 = \dfrac{1}{\sqrt{g}}\partial_u\left[\sqrt{g}\left(\kappa^u_l g^{lv} + T(S^{\mathrm{T}})^u_k\sigma^k_l S^l_i g^{iv} + T(S^{\mathrm{T}})^u_k\sigma^k_l g^{lv}\right)\partial_v T\right] \\ \quad + (\partial_u\mu)\left(\sigma^u_l g^{lv}\partial_v\mu + \sigma^u_k S^k_l g^{lv}\partial_v T\right), \end{cases} \tag{4}$$

where indexes u, l, v, k, i, v take 1, 2, 3 and g is the determinant of the matrix $g_{ij}\left(g_{ij} = \frac{\partial x^{i'}}{\partial x^i}g_{i'j'}\frac{\partial x^{j'}}{\partial x^j} = (\boldsymbol{A}\boldsymbol{A}^{\mathrm{T}})^{-1}\right)$, thus resulting in $\sqrt{g} = \det{}^{-1}(\boldsymbol{A})$. Note that we here take the second-order tensor in this form M^u_v on the basis of $\boldsymbol{g}^u$ and $\boldsymbol{g}^v$, which can be transformed into $M^{uv} = M^u_l g^{lv}$ on the basis of $\boldsymbol{g}^u$ and $\boldsymbol{g}^v$.

For the sake of explanation, we start from a known shape (the red line in Figure 1A) of the isotherm $T(x^{1'}, x^{2'}, x^{3'})$ (the same as the isopotential line $\mu(x^{1'}, x^{2'}, x^{3'})$) in the Cartesian coordinates with given parameters $\kappa^{u'}_{v'}$, $\sigma^{u'}_{v'}$, and $S^{u'}_{v'}$, satisfying

$$\begin{cases} 0 = \partial_{u'}\left(\sigma^{u'}_{v'}\partial_{v'}\mu + \sigma^{u'}_{k'}S^{k'}_{v'}\partial_{v'}T\right), \\ 0 = \partial_{u'}\left[\left(\kappa^{u'}_{v'} + T(S^{\mathrm{T}})^{u'}_{k'}\sigma^{k'}_{l'}S^{l'}_{v'} + T(S^{\mathrm{T}})^{u'}_{k'}\sigma^{k'}_{v'}\right)\partial_{v'}T\right] \\ \quad + (\partial_{u'}\mu)\left[\sigma^{u'}_{v'}\partial_{v'}\mu + \sigma^{u'}_{k'}S^{k'}_{v'}\partial_{v'}T\right]. \end{cases} \tag{5}$$

Assume that the isotherm shape presented in Figure 1B meets our expectation, we then introduce a coordinate transformation,

$$\begin{aligned} x^1 &= x^{1'}\cos x^{2'}, \\ x^2 &= x^{1'}\sin x^{2'}, \\ x^3 &= x^{3'}, \end{aligned} \tag{6}$$

where the domain equation can be described by Equation (4). Because there is only coordinate transformation from Figure 1A to B, the constitutive parameters in the curvilinear coordinates can be expressed as

$$\begin{cases} \kappa^u_v = A^u_{u'}\kappa^{u'}_{v'}A^v_{v'}, \\ \sigma^u_v = A^u_{u'}\sigma^{u'}_{v'}A^v_{v'}, \\ S^u_v = A^u_{u'}S^{u'}_{v'}A^v_{v'}, \end{cases} \tag{7}$$

where the indices u and v can be replaced by any other indices. Substituting Equation (7) into Equation (4), the component form of the domain equation in the curvilinear coordinates can be rewritten as

$$\begin{cases} 0 = \partial_u\left[\frac{1}{\det(\mathbf{A})}\left(A^u_{u'}\sigma^{u'}_{v'}A^v_{v'}\partial_v\mu + A^u_{u'}\sigma^{u'}_{k'}S^{k'}_{v'}A^v_{v'}\partial_v T\right)\right], \\ 0 = \partial_u\left[\frac{A^u_{u'}}{\det(\mathbf{A})}\left(\kappa^{u'}_{v'} + T(S^{\mathrm{T}})^{u'}_{k'}\sigma^{k'}_{l'}S^{l'}_{v'} + T(S^{\mathrm{T}})^{u'}_{k'}\sigma^{k'}_{v'}\right)A^v_{v'}\partial_v T\right] \\ \quad + \frac{1}{\det(\mathbf{A})}(\partial_u\mu)\left(A^u_{u'}\sigma^{u'}_{v'}A^v_{v'}\partial_v\mu + A^u_{u'}\sigma^{u'}_{k'}S^{k'}_{v'}A^v_{v'}\partial_v T\right). \end{cases} \tag{8}$$

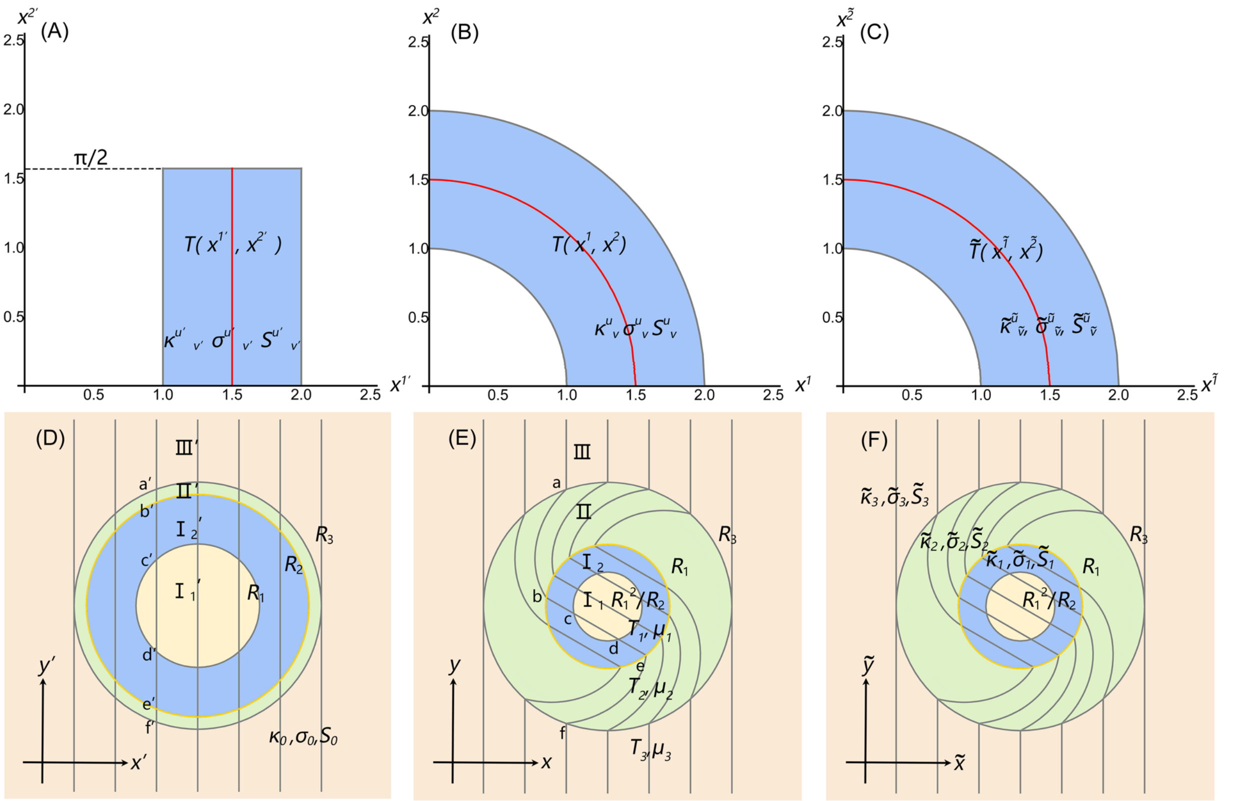

FIGURE 1 Schematic diagram of the coordinate transformation process in cylinder structure. (A), (D), (C), and (F) Cartesian coordinates. (B) and (E) Curvilinear coordinates. The red lines denote isotherms. From (A), (D) to (B), (E): only coordinate transformation. From (A), (D) to (C), (F): only constitutive parameters' transformation. The isotherm shape in (C) and (F) is the same as that in (B) and (E), indicating that the effect of parameters' transformation is equivalent to coordinate transformation.

It is worth mentioning that these two coordinates describe the same temperature distribution ($T(x^{1'}, x^{2'}, x^{3'}) = T(x^1, x^2, x^3)$), although the isotherm shape in the curvilinear coordinates is different from that in the Cartesian coordinates. In other words, the shape plotted in the curvilinear coordinates is virtual, requiring us to retain the equivalent shape in the Cartesian coordinates (Figure 1C). As we know, two factors determining the field distributions are boundary conditions and the governing equations. Therefore, we look for a new set of parameters $\tilde{\kappa}^{\tilde{u}}_{\tilde{v}}$, $\tilde{\sigma}^{\tilde{u}}_{\tilde{v}}$, and $\tilde{S}^{\tilde{u}}_{\tilde{v}}$ in the Cartesian coordinates to match Equation (8). The dominant equation of the temperature $\tilde{T}(x^{\tilde{1}}, x^{\tilde{2}}, x^{\tilde{3}})$can be easily expressed as

$$\begin{cases} 0 = \partial_{\tilde{u}}\left(\tilde{\sigma}^{\tilde{u}}_{\tilde{v}}\partial_{\tilde{v}}\tilde{\mu} + \tilde{\sigma}^{\tilde{u}}_{\tilde{k}}\tilde{S}^{\tilde{k}}_{\tilde{v}}\partial_{\tilde{v}}\tilde{T}\right), \\ 0 = \partial_{\tilde{u}}\left[\left(\tilde{\kappa}^{\tilde{u}}_{\tilde{v}} + \tilde{T}(\tilde{S}^{\mathrm{T}})^{\tilde{u}}_{\tilde{k}}\tilde{\sigma}^{\tilde{k}}_{\tilde{l}}\tilde{S}^{\tilde{l}}_{\tilde{v}} + \tilde{T}(\tilde{S}^{\mathrm{T}})^{\tilde{u}}_{\tilde{k}}\tilde{\sigma}^{\tilde{k}}_{\tilde{v}}\right)\partial_{\tilde{v}}\tilde{T}\right] \\ \quad + (\partial_{\tilde{u}}\tilde{\mu})\left[\tilde{\sigma}^{\tilde{u}}_{\tilde{v}}\partial_{\tilde{v}}\tilde{\mu} + \tilde{\sigma}^{\tilde{u}}_{\tilde{k}}\tilde{S}^{\tilde{k}}_{\tilde{v}}\partial_{\tilde{v}}\tilde{T}\right], \end{cases} \tag{9}$$

by taking $g^{\tilde{i}\tilde{j}} = \delta_{\tilde{i}\tilde{j}}$ and $\sqrt{g} = 1$. As long as the forms of Equations (8) and (9) are consistent and the corresponding boundary conditions are satisfied, then the isotherm shape in the curvilinear coordinates (Figure 1B) would be realized in the Cartesian coordinates (Figure 1C). Due to the equivalence between x^u and $x^{\tilde{u}}$, one can obtain transformation relations of constitutive parameters, $\tilde{\kappa}^{\tilde{u}}_{\tilde{v}} = A^u_{u'}\kappa^{u'}_{v'}A^v_{v'}/\det(\boldsymbol{A})$, $\tilde{\sigma}^{\tilde{u}}_{\tilde{v}} = A^u_{u'}\sigma^{u'}_{v'}A^v_{v'}/\det(\boldsymbol{A})$, and $\tilde{S}^{\tilde{u}}_{\tilde{v}} = A^{u'}_{u}S^{u'}_{v'}A^v_{v'}$. As we usually discuss these tensors on the contravariant basis of $\boldsymbol{g}^{\tilde{u}}$and $\boldsymbol{g}^{\tilde{v}}$, they should be transformed by the metric of the Cartesian coordinates, for example, $\kappa^{\tilde{u}\tilde{v}} = \kappa^{\tilde{u}}_{\tilde{i}}\delta^{\tilde{i}\tilde{v}} = \kappa^{\tilde{u}}_{\tilde{v}}$. Then, we rewrite the transformation relation as $\tilde{\kappa}^{\tilde{u}\tilde{v}} = A^u_{u'}\kappa^{u'v'}A^v_{v'}/\det(\boldsymbol{A})$, $\tilde{\sigma}^{\tilde{u}\tilde{v}} = A^u_{u'}\sigma^{u'v'}A^v_{v'}/\det(\boldsymbol{A})$, and $\tilde{S}^{\tilde{u}\tilde{v}} = A^{u'}_{u}S^{u'v'}A^v_{v'}$, which can be reduced to the matrix form,

$$\begin{cases} \tilde{\boldsymbol{\kappa}} = \dfrac{\boldsymbol{A}\boldsymbol{\kappa}'\boldsymbol{A}^{\mathrm{T}}}{\det(\boldsymbol{A})}, \\ \tilde{\boldsymbol{\sigma}} = \dfrac{\boldsymbol{A}\boldsymbol{\sigma}'\boldsymbol{A}^{\mathrm{T}}}{\det(\boldsymbol{A})}, \\ \tilde{\boldsymbol{S}} = \boldsymbol{A}^{-\mathrm{T}}\boldsymbol{S}'\boldsymbol{A}^{\mathrm{T}}, \end{cases} \tag{10}$$

which guarantees the invariance of the TE coupling equation after a coordinate transformation and guides us to design a series of thermal metamaterials.

3 | RESULTS

3.1 | TE rotating concentrator and cloak

There are two typical aspects for manipulating heat flux (or electric current): density and direction. For example, thermal concentrators can enhance the area of heat flux in a given region, and thermal rotators can change the direction of heat flux. Here, we take these two functions into account in a device. As shown in Figure 1D, the space in Cartesian coordinates is artificially divided into four regions with the same thermal conductivity κ_0, electrical conductivity σ_0, Seebeck coefficient S_0: Region I_1' ($r' < R_1$); Region I_2' ($R_1 < r' < R_2$); Region II$'$ ($R_2 < r' < R_3$); and Region III$'$ ($r' > R_3$). Then, we perform the following coordinate transformation for these regions,

$$\begin{cases} r = \frac{R_1}{R_2} r', \\ \theta = \theta' + \theta_0, \end{cases} (0 < r' < R_2) \tag{11}$$

$$\begin{cases} r = \frac{(R_3 - R_1)r' + (R_1 - R_2)R_3}{R_3 - R_2}, \\ \theta = \theta' + \frac{r - R_3}{R_2 - R_3}\theta_0, \end{cases} (R_2 < r' < R_3) \tag{12}$$

$$\begin{cases} r = r', \\ \theta = \theta'. \end{cases} (r' > R_3) \tag{13}$$

Here, R_2 ranges from 0 to R_3, yielding three different devices: rotating the imperfect (perfect) cloak for $R_2 < R_1 (R_2 = 0)$; the rotator for $R_2 = R_1$; and the rotating concentrator for $R_1 < R_2 < R_3$. By such transformation, we can compress and rotate the temperature (or voltage) distribution of Regions I_1' and I_2' without disturbing the physical fields of the background (Region III$'$). Figure 1E shows that the isotherm $a' - b' - c' - d' - e' - f'$ (or isopotential line) changes into the shape of curve $a - b - c - d - e - f$ after a coordinate transformation. The Jacobian transformation matrix of Equations (11)–(13) can be calculated by

$$\mathbf{A} = \begin{pmatrix} \partial r/\partial r' & \partial r/(r'\partial\theta') \\ r\partial\theta/\partial r' & r\partial\theta/(r'\partial\theta') \end{pmatrix}. \tag{14}$$

Substituting Equation (14) into Equation (10), we can obtain the spatial distribution of material parameters (Figure 1F),

$$\begin{cases} \tilde{\kappa}_1 = \tilde{\kappa}_3 = \kappa_0 \\ \tilde{\kappa}_2 = \mathbf{M}\kappa_0 \end{cases}, \begin{cases} \tilde{\sigma}_1 = \tilde{\sigma}_3 = \sigma_0 \\ \tilde{\sigma}_2 = \mathbf{M}\sigma_0 \end{cases}, \tilde{S}_1 = \tilde{S}_2 = \tilde{S}_3 = S_0. \tag{15}$$

The transformation matrix is presented as follows:

$$\mathbf{M} = \begin{bmatrix} m_{\tilde{r}\tilde{r}} & m_{\tilde{r}\tilde{\theta}} \\ m_{\tilde{\theta}\tilde{r}} & m_{\tilde{\theta}\tilde{\theta}} \end{bmatrix}, \tag{16}$$

where

$$\begin{aligned} m_{\tilde{r}\tilde{r}} &= 1 + \frac{(R_1 - R_2)R_3}{(R_2 - R_3)\tilde{r}}, \\ m_{\tilde{r}\tilde{\theta}} = m_{\tilde{\theta}\tilde{r}} &= \frac{[R_3\tilde{r} + R_2(R_3 - \tilde{r}) - R_1R_3]\theta_0}{(R_2 - R_3)(R_3 - R_1)}, \\ m_{\tilde{\theta}\tilde{\theta}} &= \frac{(R_3 - R_2)\tilde{r}}{R_3 r + R_2(R_3 - \tilde{r}) - R_1R_3} + \frac{[R_3 r + R_2(R_3 - \tilde{r}) - R_1R_3]\theta_0^2\tilde{r}}{(R_1 - R_3)^2(R_3 - R_2)}. \end{aligned} \tag{17}$$

To confirm the designed TE rotating concentrator and cloak, finite-element simulations with the commercial software COMSOL Multiphysics are performed. In COMSOL, we use two templates: heat transfer in solids and electric current. Without loss of generality, we consider a core−shell structure embedded in a finite background with uniform gradient physical fields (∇T_0 and $\nabla\mu_0$). These external fields are generated by setting the left and right boundary at constant T_L (μ_L) and T_R (μ_R), respectively. Figure 2 shows the simulation results of rotating metamaterials. It is clear that the density of heat flux (or electric current) is enhanced, and the direction of heat flux is rotated by a certain angle for panels Figure 2A1,B1. On the contrary, Figure 2A3,C3 shows that the TE rotating imperfect cloak can reduce (rotate) the density (direction) of heat flux and electric current without disturbing background physical fields. For comparison, we also simulate the TE rotator (Figure 2A2,B2) by setting R_2 to R_1. To see the angle of rotation more clearly, we plot the polar diagram (Figure 2A4,B4) of temperature and voltage in different boundaries (BDs), where the arrows represent the direction of heat flux or electric current.

3.2 | Temperature-switching TE rotating concentrator cloak

The above discussion is based on linear materials, for which thermal conductivity is independent of temperature. However, nonlinearity phenomena are common, and their underlying mechanisms are significant for understanding and designing complex systems. Generally, the thermal conductivities of natural materials are basically dependent on temperature (nonlinear), which provides a hint for function switching at different temperatures. Inspired by this concept, we introduce temperature into geometrical transformation relations,

$$R_2 = \frac{R_3}{1 + \mathrm{Exp}[\alpha(T - T_c)]}, \tag{18}$$

where T_c is a critical point and α is a scaling coefficient for ensuring the step change around T_c. By combining Equations (15) and (18), we can obtain temperature-dependent thermal and electric conductivities. Without changing the external voltage (μ_L and μ_R), the TE rotating cloak (Figure 3A1,B1) and concentrator (Figure 3A2,B2) are, respectively, realized when $T > T_c$ and $T < T_c$. This device switches between the two functions as the temperature jumps near the critical value. Similarly, polar diagrams in Figure 3A3,B3 show that this device can rotate the heat flow and electric current by a predetermined angle.

3.3 | Electrically controlled TE rotating concentrator

In addition, the external voltage is another manipulating method for temperature distribution. We first solve the temperature field before transformation by introducing a generalized auxiliary potential $U = \mu + ST$,[33] and then, Equation (3) reduces to

$$\begin{cases} \sigma\nabla^2 U = 0, \\ \kappa\nabla^2 T = \sigma\nabla U \cdot \nabla U. \end{cases} \tag{19}$$

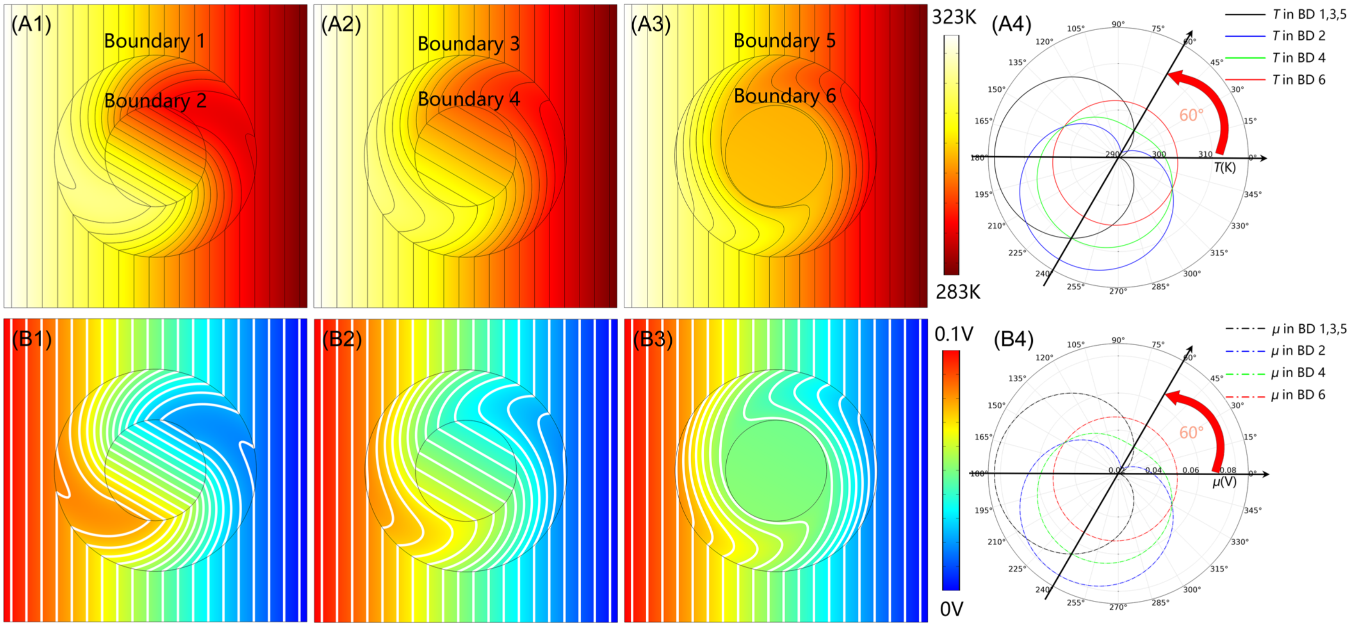

FIGURE 2 Simulative results of the (A1) (B1) rotating cloak, (A2) (B2) rotator, and (A3) (B3) rotating concentrator. (A4) and (B4), respectively, denote the temperature and voltage distribution along the corresponding boundary (BD). The black arrows represent the directions of heat flux and electric current. Parameters: (A1), (B1) R_2 = 3.8 cm; (A2), (B2) R_2 = 2 cm; (A3), (B3) R_2 = 0.2 cm; and (A1)–(B3) R_1 = 2 cm, R_3 = 4 cm, T_L = 323 K, T_R = 283 K, μ_L = 0.1 V, μ_R = 0 V, background size 12 × 12 cm^2, θ_0 = 60°, κ_0 = 100W m^{-1} K^{-1}, σ_0 = 10^4 S m^{-1}, S_0 = 3 × 10^{-4} V K^{-1}, and $\tilde{\kappa}_1$, $\tilde{\kappa}_2$, $\tilde{\kappa}_3$, $\tilde{\sigma}_1$, $\tilde{\sigma}_2$, $\tilde{\sigma}_3$, $\tilde{S}_1$, $\tilde{S}_2$, and $\tilde{S}_3$ can be calculated by Equation (15).

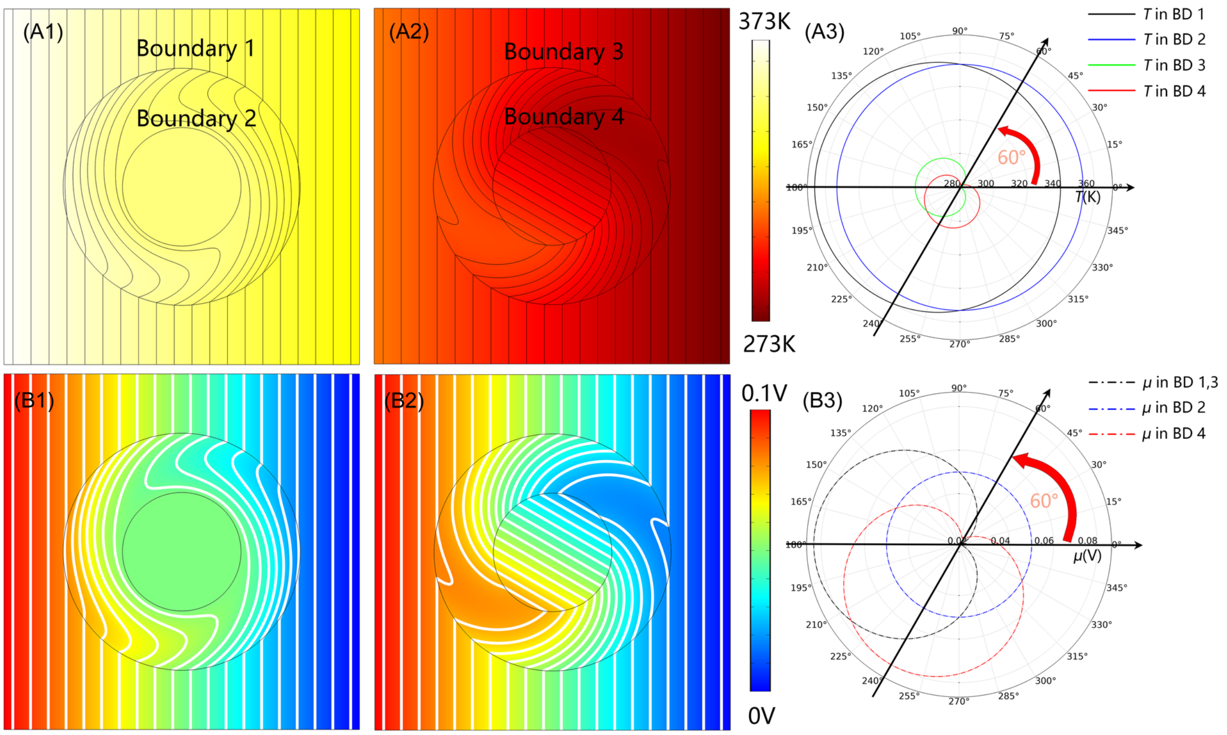

FIGURE 3 Simulative results of the TE rotating cloak concentrator under different external temperatures ($T_L$and T_R). (A1) (A2), respectively, present the temperature fields of this device at high and low temperatures. (B1) (B2), respectively, present the voltage fields of this device at high and low temperatures. (A3) (B3), respectively, illustrate the temperature and voltage distribution along the corresponding boundary. The black arrows represent the directions of heat flux and electric current. Parameters: (A1)–(A3) T_L = 373 K and T_R = 333 K; (B1)–(B3) T_L = 313 K and T_R = 273 K; and (A1)–(C3) R_1 = 2 cm, R_3 = 4 cm, $R_2 = R_3/[1 + \exp(\alpha(T - T_c))]$, α = 5, T_c = 323 K, μ_L = 0.1 V, μ_R = 0 V, background size 12 × 12 cm^2, θ_0 = 60°, κ_0 = 100 W m^{-1} K^{-1}, σ_0 = 10^4 S m^{-1}, S_0 = 3 × 10^{-4} V K^{-1}, and $\tilde{\kappa}_1$, $\tilde{\kappa}_2$, $\tilde{\kappa}_3$, $\tilde{\sigma}_1$, $\tilde{\sigma}_2$, $\tilde{\sigma}_3$, $\tilde{S}_1$, $\tilde{S}_2$, and $\tilde{S}_3$can be determined by Equations (15) and (18).

The first equation is the Laplace equation with respect to U, which can be easily calculated from

$$U = \frac{U_R - U_L}{L}x' + \frac{U_R + U_L}{2}, = \frac{S(T_R - T_L) + \mu_R - \mu_L}{L}x' + \frac{S(T_R + T_L) + \mu_R + \mu_L}{2}. \tag{20}$$

The latter is a Poisson equation, which has the particular solution,

$$T = \frac{-\sigma U^2}{2\kappa} = \frac{L(T_L + T_R) + 2(T_R - T_L)x'}{2L} + \frac{\sigma[S(T_L - T_R) + \mu_L - \mu_R]^2(L^2 - 4x'^2)}{8\kappa L^2}, \tag{21}$$

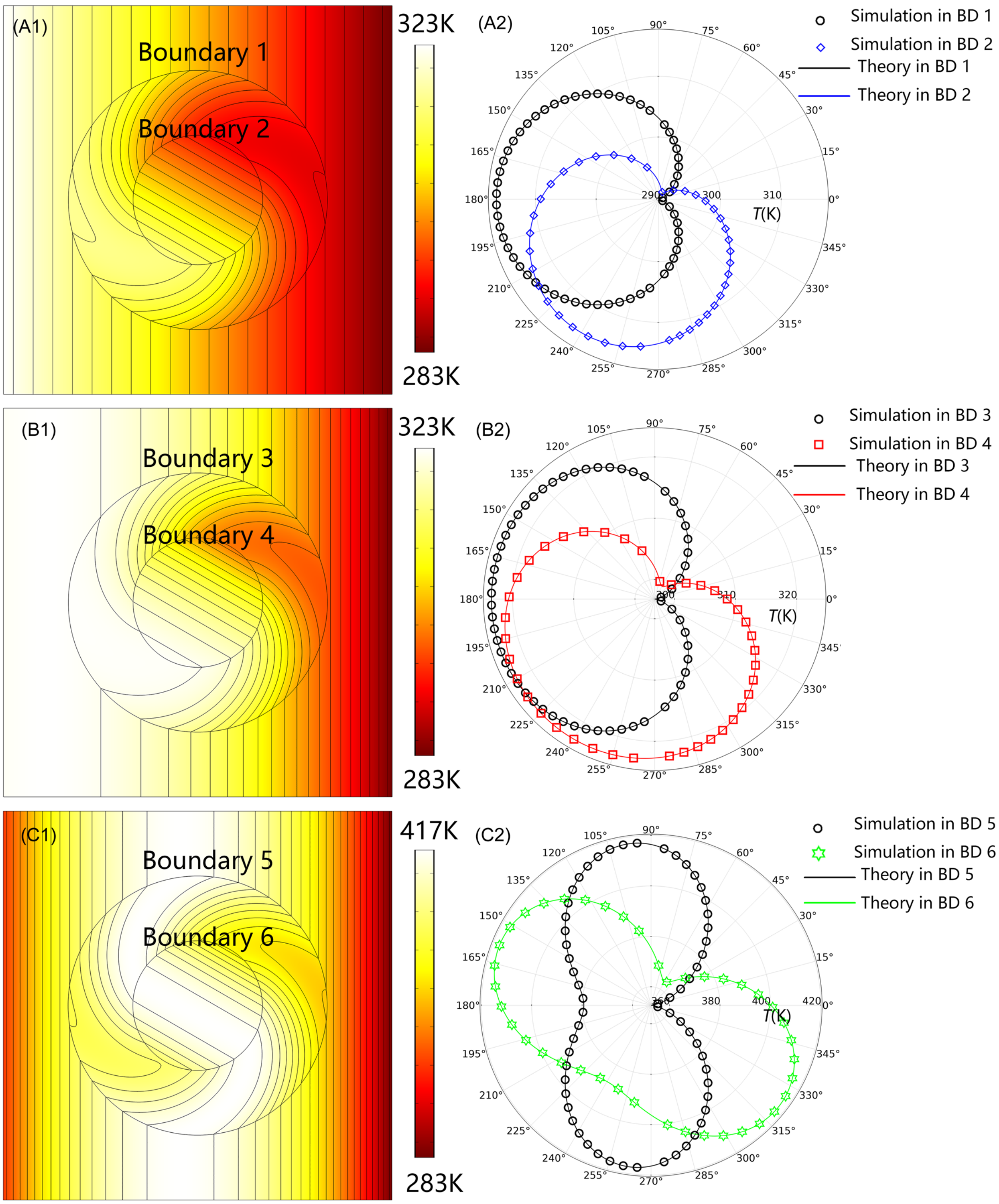

FIGURE 4 (A1), (B1), (C1) Temperature fields of the TE rotating concentrator under different external voltages (μ_L and μ_R). (A2), (B2), (C2) present the temperature distribution along the corresponding boundary. The continuous lines are predicted by Equation (23), while the scatters denote simulated results. Parameters: (A1), (A2) $\mu_L = 0.1$ V; (B1), (B2) $\mu_L = 1$ V; (C1), (C2) $\mu_L = 3$ V; (A1)–(C2) $R_1 = 2$ cm, $R_2 = 3.8$ cm, $R_3 = 4$ cm, $T_L = 373$ K, $T_R = 273$ K, $\mu_R = 0$ V, background size $12 \times 12\,\text{cm}^2$, $\theta_0 = 60°$, $\kappa_0 = 100\,\text{W m}^{-1}\,\text{K}^{-1}$, $\sigma_0 = 10^4\,\text{S m}^{-1}$, $S_0 = 3 \times 10^{-4}\,\text{V K}^{-1}$, and $\tilde{\kappa}_1, \tilde{\kappa}_2, \tilde{\kappa}_3, \tilde{\sigma}_1, \tilde{\sigma}_2, \tilde{\sigma}_3, \tilde{S}_1, \tilde{S}_2$, and $\tilde{S}_3$ can be calculated by Equation (15).

where the first term is generated by external heat sources and the other term is generated by the TE effect. So far, we have derived the temperature distribution before the coordinate transformation. Then, we substitute the transformation relation (equivalent to Equations 11 and 13),

$$\begin{cases} x' = \dfrac{R_2[\cos(\theta_0) + \sin(\theta_0)y]}{R_1}, & (r' < R_2) \\ y' = \dfrac{R_2[-\sin(\theta_0)x + \cos(\theta_0)y]}{R_1}, & \end{cases}, \quad \begin{cases} x' = x, (r' > R_3) \\ y' = y, \end{cases} \tag{22}$$

into Equation (21), and the temperature distributions of the core and background can be written as

$$\begin{cases} T_1 = \dfrac{L(T_L + T_R) + 2(T_R - T_L)\left(\dfrac{R_2[\cos(\theta_0)x + \sin(\theta_0)y]}{R_1}\right)}{2L} \\ \quad + \dfrac{\sigma[S(T_L - T_R) + \mu_L - \mu_R]^2 \left[L^2 - 4\left(\dfrac{R_2[\cos(\theta_0)x + \sin(\theta_0)y]}{R_1}\right)^2\right]}{8\kappa L^2}, \\ T_3 = \dfrac{L(T_L + T_R) + 2(T_R - T_L)x}{2L} \\ \quad + \dfrac{\sigma[S(T_L - T_R) + \mu_L - \mu_R]^2(L^2 - 4x^2)}{8\kappa L^2}. \end{cases} \tag{23}$$

Clearly, the correlation between temperature and the external electric voltage leads to an approach to regulate the thermal field further. To demonstrate the effect of the external electric voltage, we keep the external thermal field (T_L and T_R) constant. When the difference in external voltage is low, the TE effect can be ignored, so the temperature distribution is regulated only by the transformation theory (Figure 4A1). When the difference increases, the TE effect increases gradually, heating all regions (Figure 4B1). When the difference is relatively high, the TE effect dominates, even leading to a maximum temperature higher than that of external sources (Figure 4C1). The temperature field excited by the TE effect is a quadratic function, so the core region ($x = 0$) is heated up the most. In addition, this effect can be preserved in the process of coordinate transformation, that is, concentration and rotation. To further validate the calculation, we compare the simulated temperature distribution along different boundaries with theoretical predictions (Figure 4A2–C2). Obviously, the simulated curves coincide well with the prediction (scatter points) of Equation (23).

4 | DISCUSSION AND CONCLUSION

In this work, we investigate the TE field by two methods: coordinate transformation and solving the TE coupling equation directly. Both methods yield analytical solutions for physical fields, which guarantees the consistency of the simulation results (Figures 2–4) and theoretical predictions. Nevertheless, these metamaterials based on the transformation theory usually require extreme constitutive parameters, such as anisotropy, inhomogeneity, or even singularity, thus limiting the practical applications. Fortunately, the effective medium theory can provide the possibility of complicated parameters. For example, we can design the spatial distribution of two natural materials to achieve the desired spatial distribution of anisotropic thermal conductivity. In addition, the temperature-switching TE rotating concentrator cloak requires thermal (electric) conductivity varying with temperature as a step function, which can be solved by shape memory alloys.[46,47] As the alloy's temperature changes, the bimetallic strip is driven up and down, yielding decreased and increased thermal (electric) conductivity. Although this study focuses on steady-state TE transport, it could be extended to transient cases by considering the effects of density and heat capacity.

In summary, we prove the invariance of the TE coupling equation under coordinate transformation, deriving the transformation relations of constitutive parameters. Using this relationship, we design the TE rotating concentrator and cloak. The former can enhance the density of heat flux (electric current) and rotate its direction simultaneously, while the latter can realize the opposite function. To further manipulate the TE field, we introduce an additional degree of freedom, temperature, into the design of the metamaterial. Utilizing the temperature-dependent thermal (electric) conductivity, we realize the temperature-switching TE rotating concentrator cloak, which can switch between functions near the critical temperature. In addition, the TE effect of external voltage is significant for temperature control. Therefore, we calculate the general solution of temperature and design an electrically controlled TE rotating concentrator. These schemes are simulated in COMSOL Multiphysics, demonstrating the validity of our theoretical predictions. Our results can be extended to a transient case and may have potential applications for thermal management.

ACKNOWLEDGMENTS

The authors acknowledge financial support from the National Natural Science Foundation of China (No. 12035004) and from the Science and Technology Commission of Shanghai Municipality (No. 20JC1414700).

CONFLICT OF INTEREST STATEMENT

The authors declare no conflict of interest.

DATA AVAILABILITY STATEMENT

All data needed to evaluate the conclusions in the paper are available in the paper. Additional data related to this paper may be requested from the authors.

ORCID

Jiping Huang http://orcid.org/0000-0002-3617-3275

REFERENCES

1. Fan CZ, Gao Y, Huang JP. Shaped graded materials with an apparent negative thermal conductivity. *Appl Phys Lett*. 2008;92(25):251907.

2. Yang S, Wang J, Dai GL, Yang FB, Huang JP. Controlling macroscopic heat transfer with thermal metamaterials: theory, experiment and application. *Phys Rep*. 2021;908:1-65.
3. Li Y, Li W, Han TC, et al. Transforming heat transfer with thermal metamaterials and devices. *Nat Rev Mater*. 2021;6(6):488-507.
4. Guenneau S, Amra C. Anisotropic conductivity rotates heat fluxes in transient regimes. *Opt Express*. 2013;21(5):6578-6583.
5. Yang FB, Tian BY, Xu LJ, Huang JP. Experimental demonstration of thermal chameleonlike rotators with transformation-invariant metamaterials. *Phys Rev Appl*. 2020;14(5):054024.
6. Yu GX, Lin YF, Zhang GQ, Yu Z, Yu LL, Su J. Design of square-shaped heat flux cloaks and concentrators using method of coordinate transformation. *Front Phys*. 2011;6(1):70.
7. Guenneau S, Amra C, Veynante D. Transformation thermodynamics: cloaking and concentrating heat flux. *Opt Express*. 2012;20(7):8207-8218.
8. Chen F, Lei DY. Experimental realization of extreme heat flux concentration with easy-to-make thermal metamaterials. *Sci Rep*. 2015;5(1):1-8.
9. Xu GQ, Zhang HC, Jin Y. Achieving arbitrarily polygonal thermal harvesting devices with homogeneous parameters through linear mapping function. *Energy Convers Manage*. 2018;165:253-262.
10. Ji QX, Fang GD, Liang J. Achieving thermal concentration based on fiber reinforced composite microstructures design. *J Phys D Appl Phys*. 2018;51(31):315304.
11. Xu GQ, Zhou X, Liu ZJ. Converging heat transfer in completely arbitrary profiles with unconventional thermal concentrator. *Int Commun Heat Mass Transf*. 2019;108:104337.
12. Zhuang PF, Xu LJ, Tan P, Ouyang XP, Huang JP. Breaking efficiency limit of thermal concentrators by conductivity couplings. *Sci China Phys Mech Astron*. 2022;65(11):117007.
13. Narayana S, Sato Y. Heat flux manipulation with engineered thermal materials. *Phys Rev Lett*. 2012;108(21):214303.
14. Lan CW, Li B, Zhou J. Simultaneously concentrated electric and thermal fields using fan-shaped structure. *Opt Express*. 2015;23(19):24475-24483.
15. Chen TY, Weng CN, Tsai YL. Materials with constant anisotropic conductivity as a thermal cloak or concentrator. *J Appl Phys*. 2015;117(5):054904.
16. Fujii G, Akimoto Y. Cloaking a concentrator in thermal conduction via topology optimization. *Int J Heat Mass Transf*. 2020;159:120082.
17. Ji QX, Chen XY, Liang J, et al. Designing thermal energy harvesting devices with natural materials through optimized microstructures. *Int J Heat Mass Transf*. 2021;169:120948.
18. Wegener M. Metamaterials beyond optics. *Science*. 2013;342(6161):939-940.
19. Nguyen DM, Xu HY, Zhang YM, Zhang BL. Active thermal cloak. *Appl Phys Lett*. 2015;107(12):121901.
20. Yang FY, Hung FS, Yeung WS, Yang YJ. Optimization method for practical design of planar arbitrary-geometry thermal cloaks using natural materials. *Phys Rev Appl*. 2021;15(2):024010.
21. Xu LJ, Dai GL, Wang G, Huang JP. Geometric phase and bilayer cloak in macroscopic particle-diffusion systems. *Phys Rev E*. 2020;102(3):032140.
22. Sun T, Wang XH, Yang XY, Meng T, He RY, Wang YX. Design of thermal cloak and concentrator with interconnected structure. *Int J Heat Mass Transfer*. 2022;187:122568.
23. Li JX, Li Y, Li TL, Wang WY, Li LQ, Qiu CW. Doublet thermal metadevice. *Phys Rev Appl*. 2019;11(4):044021.
24. Su YS, Li Y, Yang TZ, et al. Path-dependent thermal metadevice beyond Janus functionalities. *Adv Mater*. 2021;33(4):2003084.
25. Moccia M, Castaldi G, Savo S, Sato Y, Galdi V. Independent manipulation of heat and electrical current via bifunctional metamaterials. *Phys Rev X*. 2014;4(2):021025.
26. Li TH, Yang CF, Li SB, Zhu DL, Han Y, Li ZQ. Design of a bifunctional thermal device exhibiting heat flux concentration and scattering amplification effects. *J Phys D Appl Phys*. 2019;53(6):065503.
27. Zhou LL, Huang SY, Wang M, Hu R, Luo XB. While rotating while cloaking. *Phys Lett A*. 2019;383(8):759-763.
28. Chen MY, Shen XY, Chen Z, Xu L. Realizing the multifunctional metamaterial for fluid flow in a porous medium. *Proc Natl Acad Sci USA*. 2022;119(49):e2207630119.
29. Lei M, Wang J, Dai GL, Tan P, Huang JP. Temperature-dependent transformation multiphysics and ambient-adaptive multiphysical metamaterials. *EPL*. 2021;135(5):54003.
30. Stedman T, Woods LM. Cloaking of thermoelectric transport. *Sci Rep*. 2017;7(1):6988.
31. Wang J, Shang J, Huang JP. Negative energy consumption of thermostats at ambient temperature: electricity generation with zero energy maintenance. *Phys Rev Appl*. 2019;11(2):024053.
32. Ma YG, Liu YC, Raza M, Wang YD, He SL. Experimental demonstration of a multiphysics cloak: manipulating heat flux and electric current simultaneously. *Phys Rev Lett*. 2014;113(20):205501.
33. Qu T, Wang J, Huang JP. Manipulating thermoelectric fields with bilayer schemes beyond Laplacian metamaterials. *EPL*. 2021;135(5):54004.
34. Lan CW, Bi K, Fu XJ, Li B, Zhou J. Bifunctional metamaterials with simultaneous and independent manipulation of thermal and electric fields. *Opt Express*. 2016;24(20):23072-23080.
35. Shen XY, Fang CC, Jin ZP, et al. Achieving adjustable elasticity with non-affine to affine transition. *Nat Mater*. 2021;20(12):1635-1642.
36. Li Y, Shen XY, Wu ZH, et al. Temperature-dependent transformation thermotics: from switchable thermal cloaks to macroscopic thermal diodes. *Phys Rev Lett*. 2015;115(19):195503.
37. Li Y, Shen XY, Huang JP, Ni YS. Temperature-dependent transformation thermotics for unsteady states: switchable concentrator for transient heat flow. *Phys Lett A*. 2016;380(18):1641-1647.
38. Shen XY, Li Y, Jiang CR, Huang JP. Temperature trapping: energy-free maintenance of constant temperatures as ambient temperature gradients change. *Phys Rev Lett*. 2016;117(5):055501.
39. Shen XY, Li Y, Jiang CR, Ni YS, Huang JP. Thermal cloak-concentrator. *Appl Phys Lett*. 2016;109(3):031907.
40. Su C, Xu LJ, Huang JP. Nonlinear thermal conductivities of core-shell metamaterials: rigorous theory and intelligent application. *EPL*. 2020;130(3):34001.
41. Dai GL, Shang J, Wang RZ, Huang JP. Nonlinear thermotics: nonlinearity enhancement and harmonic generation in thermal metasurfaces. *Eur Phys J B*. 2018;91:1-7.
42. Dai GL, Huang JP. Nonlinear thermal conductivity of periodic composites. *Int J Heat Mass Transfer*. 2020;147:118917.
43. Yang S, Xu LJ, Huang JP. Metathermotics: nonlinear thermal responses of core-shell metamaterials. *Phys Rev E*. 2019;99(4):042144.
44. Zhuang PF, Wang J, Yang S, Huang JP. Nonlinear thermal responses in geometrically anisotropic metamaterials. *Phys Rev E*. 2022;106(4):044203.
45. Wang J, Dai GL, Yang FB, Huang JP. Designing bistability or multistability in macroscopic diffusive systems. *Phys Rev E*. 2020;101(2):022119.
46. Chluba C, Ge W, Miranda RL, et al. Ultralow-fatigue shape memory alloy films. *Science*. 2015;348(6238):1004-1007.
47. Dye D. Shape memory alloys: towards practical actuators. *Nat Mater*. 2015;14(8):760-761.
48. Kuo DMT, Chang YC. Thermoelectric and thermal rectification properties of quantum dot junctions. *Phys Rev B*. 2010;81(20):205321.

49. Zhang ZH, Gui YS, Fu L, et al. Seebeck rectification enabled by intrinsic thermoelectrical coupling in magnetic tunneling junctions. *Phys Rev Lett*. 2012;109(3):037206.
50. Lu JC, Wang RQ, Ren J, Kulkarni M, Jiang JH. Quantum-dot circuit-QED thermoelectric diodes and transistors. *Phys Rev B*. 2019;99(3):035129.

AUTHOR BIOGRAPHIES

Pengfei Zhuang is currently a PhD candidate in the Department of Physics at Fudan University under the guidance of Prof. Jiping Huang. He received his BS degree from the Nanjing University of Aeronautics and Astronautics, China in 2020. His research interests include transformation thermotics, thermal metamaterials, and their applications.

Jiping Huang is currently a professor in the Department of Physics at Fudan University, China. He received his PhD degree in physics from the Chinese University of Hong Kong in 2003. His research interests include thermodynamics, statistical physics, and complex systems.

How to cite this article: Zhuang P, Huang J. Multiple control of thermoelectric dual-function metamaterials. *Int J Mech Syst Dyn*. 2023;3:127-135. doi:10.1002/msd2.12070